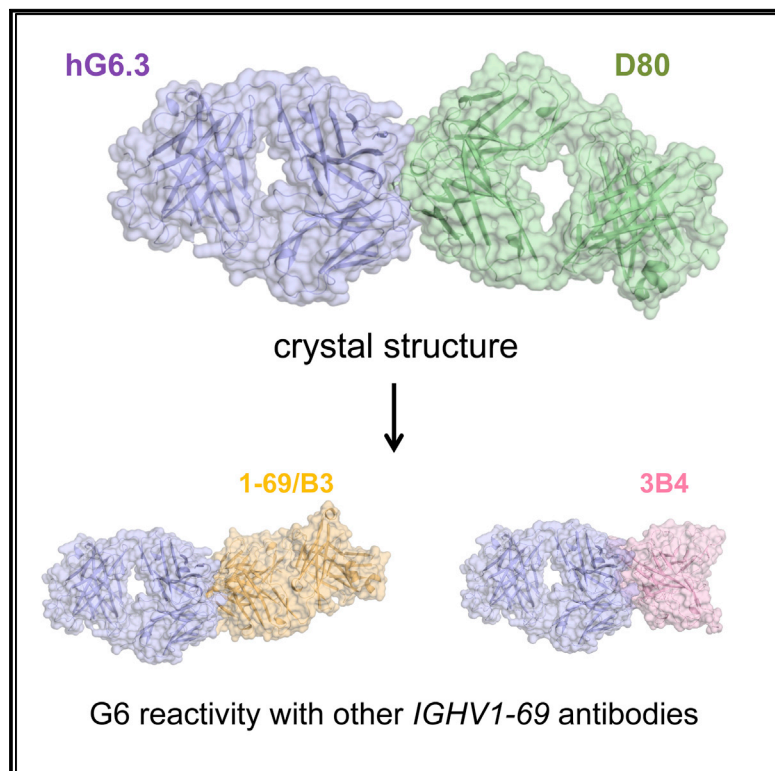# Structural Determination of the Broadly Reactive Anti-*IGHV1-69* Anti-idiotypic Antibody G6 and Its Idiotope

Graphical Abstract

Authors

Yuval Avnir, Kristina L. Prachanronarong, Zhen Zhang, ..., Nese Kurt Yilmaz, Celia A. Schiffer, Wayne A. Marasco

Correspondence

nese.kurtyilmaz@umassmed.edu (N.K.Y.),
celia.schiffer@umassmed.edu (C.A.S.),
wayne_marasco@dfci.harvard.edu (W.A.M.)

In Brief

G6 is an exceptional anti-idiotypic antibody that binds to antibodies encoded by the immunoglobulin heavy chain germline gene *IGHV1-69*. Yuval et al. describe how G6 binds to its cross-reactive idiotope by a set of binding assays and by solving the structure of humanized-G6 complexed with an *IGHV1-69*-anti-influenza Ab.

Highlights

- G6 binds to a subset of *IGHV1-69* germline-based anti-influenza Abs

- The structure of humanized G6 with a *IGHV1-69* anti-influenza Ab is reported

- Various binding assays further define the G6 cross-reactive binding idiotope

- The core binding idiotope of G6 is deduced

Data and Software Availability

5JQD
5JO4

Structural Determination of the Broadly Reactive Anti-*IGHV1-69* Anti-idiotypic Antibody G6 and Its Idiotope

Yuval Avnir,[1,2,9] Kristina L. Prachanronarong,[3,9] Zhen Zhang,[1,2,9] Shurong Hou,[3] Eric C. Peterson,[1,2] Jianhua Sui,[1,2] Hatem Zayed,[1,2] Vinodh B. Kurella,[1,2] Andrew T. McGuire,[4] Leonidas Stamatatos,[4] Brendan J. Hilbert,[3] Markus-Frederik Bohn,[3] Timothy F. Kowalik,[6] Jeffrey D. Jensen,[7] Robert W. Finberg,[5] Jennifer P. Wang,[5] Margaret Goodall,[8] Roy Jefferis,[8] Quan Zhu,[1,2] Nese Kurt Yilmaz,[3,*] Celia A. Schiffer,[3,*] and Wayne A. Marasco[1,2,10,*]

[1]Department of Cancer Immunology and Virology, Dana-Farber Cancer Institute, Boston, MA, USA
[2]Department of Medicine, Harvard Medical School, Boston, MA, USA
[3]Department of Biochemistry and Molecular Pharmacology, University of Massachusetts Medical School, Worcester, MA, USA
[4]Vaccine and Infectious Disease Division, Fred Hutchinson Cancer Research Center, Seattle, WA, USA
[5]Department of Medicine, University of Massachusetts Medical School, Worcester, MA, USA
[6]Department of Microbiology and Physiological Systems, University of Massachusetts Medical School, Worcester, MA, USA
[7]School of Life Sciences, Center for Evolution and Medicine, Arizona State University, Tempe, AZ, USA
[8]Institute of Immunology and Immunotherapy, College of Medical and Dental Sciences, University of Birmingham, Birmingham, UK
[9]These authors contributed equally
[10]Lead Contact
*Correspondence: nese.kurtyilmaz@umassmed.edu (N.K.Y.), celia.schiffer@umassmed.edu (C.A.S.), wayne_marasco@dfci.harvard.edu (W.A.M.)
https://doi.org/10.1016/j.celrep.2017.11.056

SUMMARY

The heavy chain *IGHV1-69* germline gene exhibits a high level of polymorphism and shows biased use in protective antibody (Ab) responses to infections and vaccines. It is also highly expressed in several B cell malignancies and autoimmune diseases. G6 is an anti-idiotypic monoclonal Ab that selectively binds to *IGHV1-69* heavy chain germline gene 51p1 alleles that have been implicated in these Ab responses and disease processes. Here, we determine the co-crystal structure of humanized G6 (hG6.3) in complex with anti-influenza hemagglutinin stem-directed broadly neutralizing Ab D80. The core of the hG6.3 idiotope is a continuous string of CDR-H2 residues starting with M53 and ending with N58. G6 binding studies demonstrate the remarkable breadth of binding to 51p1 *IGHV1-69* Abs with diverse CDR-H3, light chain, and antigen binding specificities. These studies detail the broad expression of the G6 cross-reactive idiotype (CRI) that further define its potential role in precision medicine.

INTRODUCTION

With the emerging field of precision medicine comes an expanding need to understand immunoglobulin (IG)-biased gene utilization at the molecular level so that vaccines with universal efficiency in the population can be deployed. In the fields of cancer and autoimmune disease, targeted immunotherapies require knowledge of antibody (Ab)-protein interactions at the molecular level. Human immunoglobulin heavy-chain (IGHV) polymorphisms are recognized as a rich source of humoral immune system diversity, and the structural importance of the heavy chain (VH) in binding interactions is well-established (Watson et al., 2017). Structural and copy-number variations in many IGHV loci can lead to wide variability in expression levels and biological activity of Abs and B cell receptors (BCRs) (Avnir et al., 2016; Watson and Breden, 2012; Watson et al., 2013).

Anti-idiotypic (anti-Id[+]) antibodies are defined as those capable of binding to the variable domains of other Abs (idiotopes) (Grey et al., 1965; Kunkel et al., 1963; Oudin and Michel, 1969a, 1969b). In 1986, Mageed et al. (1986) generated mouse anti-Id[+] G6 by immunization with a human rheumatoid factor (RF) Ab of the Wa group. G6 was shown to bind to the RF heavy chain, not to the light chain. Through sequencing VH genes of G6-reactive RFs (Newkirk et al., 1987) and G6-reactive CLL B cells (Kipps et al., 1989), it became apparent that the G6 binding idiotope is encoded by the 51p1 allele family of *IGHV1-69* germline genes (Kipps et al., 1989; Schroeder et al., 1987) that are defined by CDR-H2 Phe54 (F-alleles) as opposed to the G6 nonreactive hv1263 germline gene alleles that encode CDR-H2 Leu54 (L-alleles) (Potter et al., 1999). Currently, the International Immunogenetics Information System (IMGT) database lists 14 *IGHV1-69* alleles, eight belong to the F-allele group and six to the L-allele group that show remarkably variable distribution across different ethnic populations (Avnir et al., 2016).

The expression of the G6 cross-reactive idiotype (CRI) is well-studied (Charles et al., 2013; Potter et al., 1999). Sasso et al. (1996) first reported that *IGHV1-69* gene copy number correlates with the frequency of tonsillar B cells positively stained with G6; presence of G6-reactive cells in the mantle zones of secondary B cell follicles may be strategic for host defense (Cerutti et al., 2013). In B cell chronic lymphocytic leukemia (B-CLL)

A

B
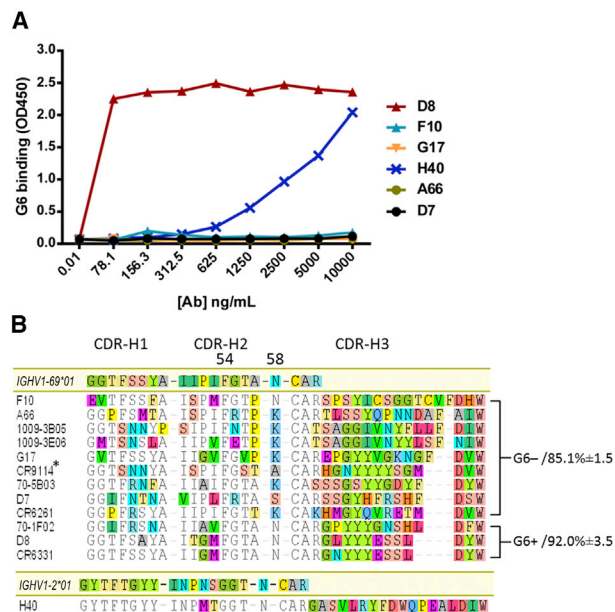
Figure 1. The G6 Idiotype Appears on Select Influenza sBnAbs

HV1-69-sBnAbs discovered in our previous study (Sui et al., 2009) were analyzed by ELISA for binding to G6 (A). Their heavy chain CDRs sequences are shown in (B) as well as other HV1-69-sBnAbs that were analyzed for G6 binding by using Biacore T100 (or by using Octet RED96 for CR9114 against hG6.3). Grey colored residues are those that are in consensus with the germline gene residues of *IGHV1-69*01* (representative of 51p1 alleles). Also shown are the residues at position 58, and the V-segment amino acid germline identity mean and SD of the G6 reactive and nonreactive groups as determined by IgBlast.

(Chang et al., 2016) two distinct subgroups of patients are defined based on the absence or presence of somatic mutations in the variable regions of the IGHV genes (Fais et al., 1998; Hashimoto et al., 1995; Schroeder and Dighiero, 1994). Patients with leukemic B cells encoding BCRs with unmutated VH genes have a distinctly more aggressive and malignant disease with much shorter survival rates (Damle et al., 1999) such as with *IGHV1-69* (Hamblin et al., 1999). Remarkably, the anti-Id[+] G6 51p1 alleles are overwhelmingly predominant in this disease (Johnson et al., 1997; Keating et al., 2003). Several other biased F-allelic *IGHV1-69* Ab responses and associations with disease processes have been reported (Chan et al., 2001; Miklos et al., 2000; Steininger et al., 2012; Tang et al., 2014; Yeung et al., 2016; Ying et al., 2015). In influenza infection, the biased use of *IGHV1-69* F-alleles in the production and serum titers of broadly neutralizing antibodies to the influenza A hemagglutinin (HA) stem domain (HV1-69-sBnAbs) occurs (Avnir et al., 2014; Pappas et al., 2014). Structurally, only the rearranged VH makes contact with HA (Dreyfus et al., 2012; Ekiert et al., 2009; Sui et al., 2009). Two influenza-related studies (Avnir et al., 2016; Wheatley et al., 2015) specifically used G6 as a genotypic marker to identify individuals who are devoid of F-alleles (i.e., L/L homozygous) and showed that they have lower HV1-69-sBnAbs in serum.

The unique anti-Id[+] properties of G6 and its potential use in the monitoring and treatment of *IGHV1-69* Ab responses and associ-

ated diseases, respectively, motivated us to comprehensively study the G6 idiotope at the atomic level. In the present study, the co-crystal structures of a potent humanized G6, hG6.3 (Chang et al., 2016), bound to HV1-69-sBnAb D80 (Sui et al., 2009), and D80 alone are reported to 2.5 Å resolution. Detailed comparative structural analysis permitted the determination of the hG6.3 idiotope. Additional binding and modeling studies of a large panel of G6-reactive Abs as well as HV1-69-sBnAbs and their variants were performed. The G6 CRI is expressed on *IGHV1-69* Abs with widely varying CDR-H3, light chains and antigen specificities. Remarkably, the G6 CRI is lost on the majority of HV1-69-sBnAbs due to critical mutations around the idiotope core at CDR-H2 Phe54 that are requisite for HA binding. These hG6.3 studies provide a precise delineation of the G6 CRI and a rationale for using hG6.3 to monitor *IGHV1-69* Ab responses to vaccination and infection and advance anti-Id[+]-based immunotherapies.

RESULTS

Defining the G6 Idiotype on IGHV1-69-Encoded Human Anti-influenza Abs Targeting the HA Stem Domain

We (Sui et al., 2009) and others (Corti et al., 2017; Pappas et al., 2014) discovered the biased use of *IGHV1-69* F-alleles in HV1-69-sBnAbs. These data led us to further investigate if these HV1-69-sBnAbs also bind to the anti-Id[+] Ab G6. Surprisingly, an ELISA assay showed that of the five previously discovered HV1-69-sBnAbs (Sui et al., 2009), only D8 strongly bound to G6 (Figure 1A). Very weak binding was also observed for the *IGHV1-2* germline-based sBnAb H40. In subsequent assays that tested G6 binding of 7 other HV1-69-sBnAbs, only CR6331 (Throsby et al., 2008) and 70-1F02 (Wrammert et al., 2011) were found to express the G6 CRI. In addition, no binding activity was observed when C9114 (Dreyfus et al., 2012) was tested for binding against humanized hG6.3 (Chang et al., 2016). Thus, of a total of 12 HV1-69-sBnAbs that were tested, only three were G6-reactive. Analysis of the three G6-reactive heavy chain CDR sequences (Figure 1B) revealed the commonality of P52aA/G substitution in CDR-H2 together with shorter CDR-H3 regions that encode three tyrosine residues at positions 97–99 (Kabat numbering). The G6-reactive HV1-69-sBnAbs maintained germline N58. Fewer amino acid substitutions occur in CDR-H1 and CDR-H2, with higher V-segment germline gene identity (92.0% ± 3.5%), for G6-reactive compared to the G6-nonreactive HV1-69-sBnAbs (85.1% ± 1.5%).

Three of these G6-nonreactive HV1-69-sBnAbs, F10, A66, and CR6261, were used to investigate the contributions of V-segment amino acid substitutions, whereby the expression of G6 idiotope was analyzed for chimeras constructed by using the *IGHV1-69* germline non-mutated V-segment and maintaining the original (wild-type; WT) CDR-H3/J and light chains. Restoration of strong G6 binding was observed for the three VH1-69/F10, VH1-69/A66, and VH1-69/CR6261 chimeras (Figure 2A) that now failed to bind HA (data not shown). This finding of reciprocal gain of G6-idiotype with loss of HA binding was unexpected. We have previously shown that a consensus motif for HV1-69-sBnAbs is composed of critical amino acid substitutions in the VH-segment together with a hydrophobic amino acid at position 53, Phe54, and properly positioned
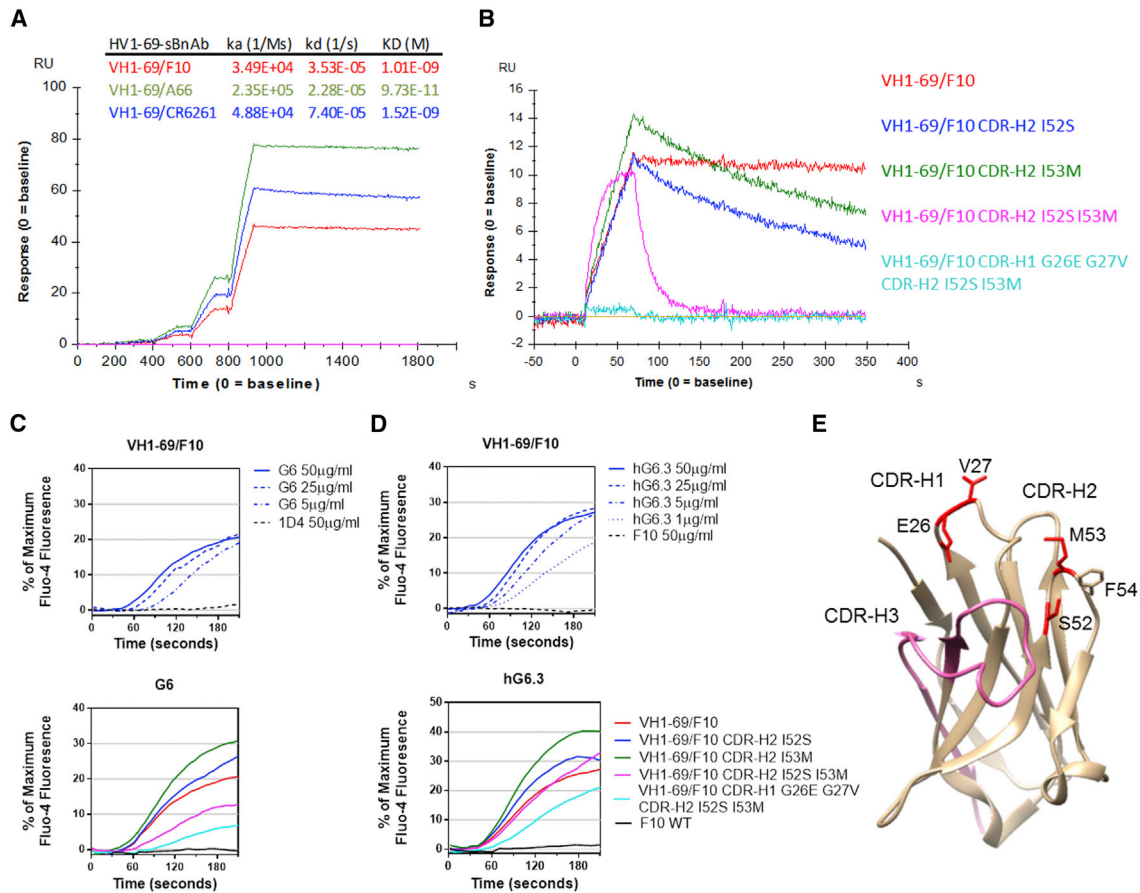
Figure 2. Analysis of G6 Idiotype by Using HV1-69-sBnAb Variants

(A) The V-segment of the non-G6 reactive HV1-69-sBnAbs F10, CR6261, and A66 was replaced with the non-mutated *IGHV1-69*01* germline V-segment. Binding kinetics of the three variants (VH1-69/F10, A66, CR6261) were analyzed against G6 by using Biacore T100.

(B) VH1-69/F10 variants were generated, in which F10's V-segment amino acid substitutions were back-introduced and then analyzed by Biacore T100 for binding activities against G6 when using a single concentration of 2.85 μg/mL per variant.

(C and D) The same variants were also tested for binding by using an artificial B cell receptor display system in which the VH1-69/F10 variants were displayed as BCRs and either G6 (C) or hG6.3 (D) were added at the concentration of 50 μg/mL. In the upper panels of (C) and (D), the binding response is shown for isotype controls and varying concentrations of G6 or h6.3 when tested against VH1-69/F10. Binding was monitored by fluorescent measurements of calcium ions being released from intracellular compartments.

(E) The heavy chain of F10 is shown (PDB 3FKU) with residues colored in red that were back-introduced in the VH1-69/F10 variants and the unchanged CDR-H3/J residues are shown in pink.

CDR-H3 Tyr (Avnir et al., 2014). Thus, unique VH-segment substitutions, particularly those involving the CDR-H2 loop, are involved in HA binding.

To further define the contribution of individual VH-segment substitutions for G6 and HA binding, several VH1-69/F10 variants were tested in which amino acid substitutions were back-introduced into CDR-H2 (Figures 2B and 2E). The substitutions of either I52S or I53M resulted in lower G6 binding affinity, as determined by faster dissociation rates, and the combined I52S I53M substitutions resulted in a significant loss in binding affinity. Interestingly, in contrast to our previous report (Avnir et al., 2014) that showed VH1-69/F10 CDR-H2 I52S restored binding activity to HA, while VH1-69/F10 CDR-H2 I53M did not, both constructs had a similar effect on diminishing G6 binding. In addition, the VH1-69/F10 CDR-H1 G26E G27V CDR-H2 I52S

I53M variant (that introduced two HV1-69-sBnAb amino acid changes in CDR-H1) resulted in complete loss of G6 binding.

This set of VH1-69/F10 variants was also displayed using artificial BCRs and tested against G6 and hG6.3 as antigens. Both G6 and hG6.3 were able to cross-link the various VH1-69/F10 variant BCRs (Figures 2C and 2D), but not the WT F10. In contrast to the kinetic binding data (Figure 2B), the VH1-69/F10 CDR-H2 I52S and VH1-69/F10 CDR-H2 I53M variants had similar and modest increases in binding, respectively, compared to VH1-69/F10, and the combination CDR-H2 and CDR-H1/H2 variants also maintained some level of G6 binding. This disparity may be attributed to avidity in the BCR experimental system that is generated by bivalent to bivalent interactions (Vauquelin and Charlton, 2013). Thus, the G6 idiotope is exclusively located in the VH segment and is most sensitive to amino acid changes
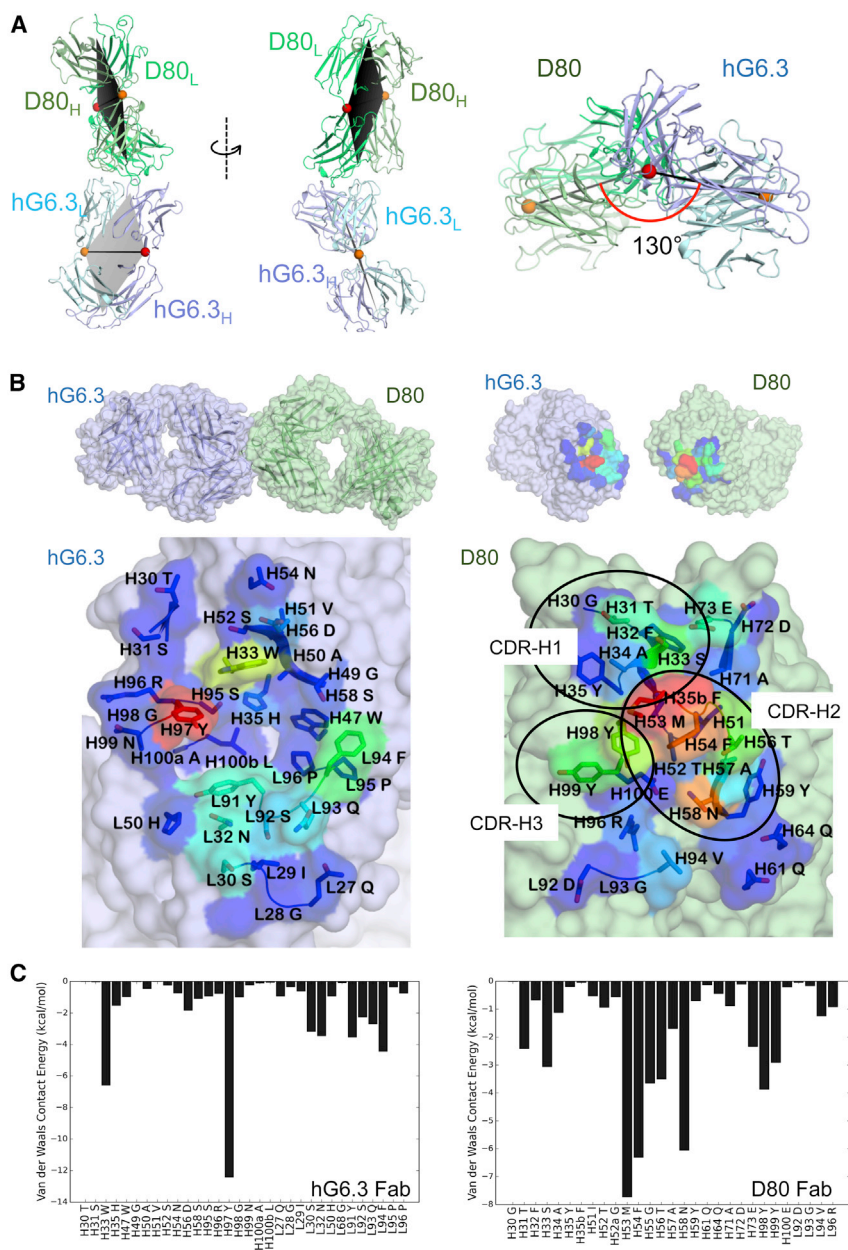
Figure 3. The Angle of Approach and Intermolecular Interactions between D80 and hG6.3

(A) The angle of approach between D80 and hG6.3, measured between the planes defined by the centers of mass for the V and C domains and the 2-fold pseudo-symmetry axis (orange and red dots) of the Fab fragments. The planes are colored lighter to darker for parallel to perpendicular relative to the image plane. The two red dots are aligned in the sight line (visual axis) in the last panel.

(B) The crystal structure of D80-hG6.3 Fab fragments splayed open to view the residues at the intermolecular interface. The residues are colored on a rainbow scale from blue to red for increasing van der Waals energy, hence warmer colors indicate residues with the most contribution to the intermolecular contacts.

(C) The intermolecular van der Waals contact energy values of residues at the interface displayed as bar graphs for hG6.3 Fab and D80 Fab.

length and height of the centroid planes (Figure 3A). The binding interface between D80 and hG6.3 has a total buried solvent-accessible surface area of 900 Å^2 per binding partner. The two antibodies interact with each other through their variable domains, where the CDR loops in the VH domain of D80 Fab directly interact with their complementary CDR loops in the VH and light chain (VL) domains of the hG6.3 Fab (Figure 3B).

## Intermolecular Binding Interface between D80 and hG6.3

To quantify the extent of interactions made by the CDRs, the intermolecular van der Waals (vdW) contact energies were calculated and mapped onto the structures of D80 and hG6.3 (see the Supplemental Experimental Procedures) (Figure 3B). Among the CDRs of D80, CDR-H2 contributes the most to the binding interface with the largest magnitude of total vdW contact energy (–7.5, –30.9, and –7.0 kcal/mol for

in CDR-H2 but can be further influenced by amino acid changes in CDR-H1.

The Crystal Structures of the D80 Fab Fragment and the D80-hG6.3 Fab Fragment Complex

The G6 idiotope was further elucidated at the structural level by investigating the critical binding interactions of one of these HV1-69-sBnAbs, D80 (that has a similar VH chain as D8 except for a K23R substitution) that binds both HA and hG6.3. The crystal structures of the Fab of D80 were determined for both D80 alone and bound to the hG6.3 Fab, each to 2.5 Å resolution (Figure 3; Table S1). Macro level view of the hG6.3-D80 complex shows that the two Abs form an angle of ~130° with respect to the

CDR-H1, -H2, and -H3, respectively), confirming that the hG6.3 binding idiotope is primarily located on CDR-H2 (red residues in Figure 3B, lower right). The residues that make the most extensive contacts with hG6.3 are M53 and F54 in CDR-H2, and at the edge, N58. The N58 side chain makes 3 intermolecular hydrogen bonds that are part of a larger hydrogen bonding network that stabilizes the bound complex across the interface (Figure 4A). A substitution at this position to cause loss of these hydrogen bonds would destabilize and likely disrupt the binding interaction. In agreement with this observation, all 3 HV1-69-sBnAbs that are G6-reactive have the germline N58. In contrast, 8 of the 9 G6-unreactive Abs have a substitution at position 58, with 6 Abs containing an N58K substitution, CR9114 having
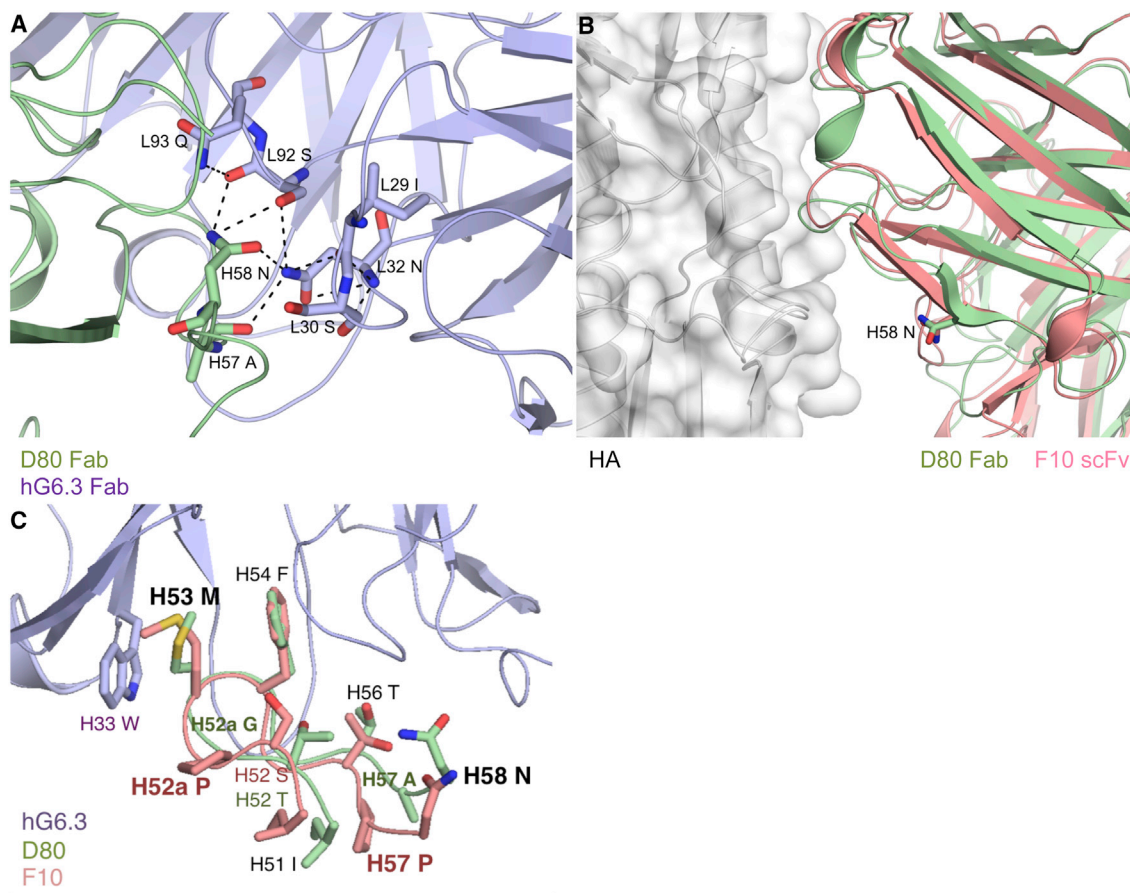
Figure 4. Position H58 N Has Extensive Interactions with hG6.3 but Not with HA

(A) D80 heavy chain Asn58 is involved in an extensive hydrogen bonding (black dashed lines) network in the D80-hG6.3 structure.

(B) Position H58 is located outside the CDR-H2 loop region, on a small beta strand following the loop and does not make any intermolecular interactions with the HA epitope in the F10-HA crystal structure. Alignment of D80 crystal structure onto F10 indicates H58 N would not be involved in any contacts with HA.

(C) Aligning the CDR-H2 F54 in F10 structure (pink) onto D80 (green), residue H58 N is positioned too far from hG6.3 (purple) to retain any intermolecular interactions across the interface due to a kink in the backbone caused by H57 P. In addition, H53 M has a side chain orientation incompatible with hG6.3's H33 W with the backbone shifting relative to D80 due to H52 P in F10.

N58A and D7 an N58S substitution. None of these substitutions would be able to retain the intermolecular side chain hydrogen bonds. Only the G6-nonreactive F10 has germline N58, this exception is discussed below. Additionally, D80 CDR-H2 residues G55 and T56 and CDR-H3 residues Y98 and Y99 also significantly contribute to the packing between the two Abs (Figure 3C, right), followed by CDR-H1 residues T31 and S33 and the framework residue E73.

In hG6.3, most of the intermolecular vdW interactions are contributed by Y97 followed by W33 of the heavy chain and F94, Y91, Q93, N32, and S30 of the light chain (Figures 3B and 3C, left). D80's M53 and F54 form a "knuckle" that inserts into a pocket with M53 and G55 extensively interacting with Y97 and W33 of the hG6.3 heavy chain and F94 packs against Y91 of the light chain. The pocket in hG6.3 where this "knuckle" inserts is not entirely filled by D80 and may play a role in the diversity of antibody binding to hG6.3. A volume of 32 Å³, as calculated by POVME (Durrant et al., 2014), lined by hydrophobic

atoms remains (Figure S1), indicating the pocket could accommodate other hydrophobic side chains.

In addition to the vdW contacts, which capture the surface-surface packing and shape complementarity at the binding interface, additional contributions by polar (hydrogen bonding) and pi-stacking interactions were analyzed to define the full hG6.3 idiotope (Figure 5; Table S2). In CDR-H1, residues T31, S33, and Y35 have side chain hydrogen bonds with VH residues W33 and D56 of hG6.3 (Figure 5A). As with vdW contacts, CDR-H2 of D80 contributes the most to the interactions with hG6: the side chain of T52, T56, and N58 of D80 have hydrogen bonds to the VL residues N32, S92, and Q93 of hG6.3. The backbone carbon of G55 in this loop is also involved in a pi-stacking interaction with Y99 of hG6.3 (Figure 5B, inset). The only polar CDR-H3 interaction is pi-stacking between VH Y99 and hG6.3 VL F94 (Figures 5C and 5D). This Tyr is part of the triple Tyr motif (Y97–Y99) that participates in an extensive pi-stacking interaction network involving CDR-H2, CDR-H3, and hG6.3 residues
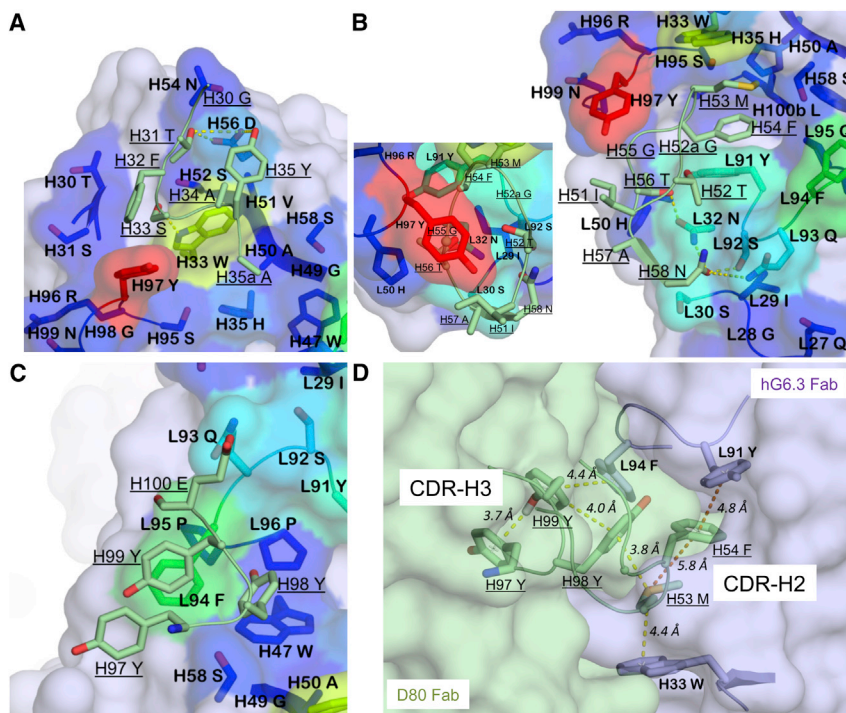
Figure 5. Hydrogen Bonding and Pi-Stacking Interactions between D80 and hG6.3

Hydrogen bonds (yellow dashes) between D80 (green sticks) and hG6.3 (purple surface) at the binding interface displayed for (A) CDR-H1 and (B) CDR-H2 (inset: pi-stacking between Y99$_H$ of hG6.3 and the backbone carbon of G55 in D80).

(C and D) CDR-H3 has no intermolecular hydrogen bonds (C) but participates in (D) an extensive pi-stacking (yellow dashes) interaction network involving the CDR-H2 and CDR-H3 of D80 (green) and hG6.3 (purple).

does not need to undergo major conformational changes for binding to occur. Hence, this similarity promises that the D80-hG6.3 crystal structure determined here can serve as an appropriate template to model the binding of other G6-reactive Abs for which unbound structures are available.

Substituting CDR-H2 F54 or N58 Has Differential Effects on hG6.3 and HA Binding

F54L substitution in an *IGHV1-69* F-allele Ab has been shown (Potter et al., 1999) to completely abolished binding to G6. To test whether D80 F54 is critical for binding, an F54L variant was engineered and binding affinity was completely abolished (Figure 6A). Molecular modeling of F54L on the hG6.3-D80 crystal structure (Figures 6C and 6D) predicted a substantial loss of intermolecular vdW contacts. Specifically, F54 aromatic ring forms extensive vdW contacts with hG6.3 light chain Y91. The smaller L54 would not reach the Y91 CB atom and thus cannot form these interactions. This decrease in vdW contacts may also affect the stability of the extensive pi-stacking interaction network involving D80 CDR-H2 and CDR-H3 (Figure 5D). In addition, L54 substitution would result in decrease of vdW contacts with light chain P96 and heavy chain H35 and S95, amounting to a total predicted loss of 5 kcal/mol in vdW contact energy. Interestingly, while G6 binding is lost with the F54L substitution, equivalent binding is still maintained against H5VN04 HA (Figure 6B). The similar binding profile of D80 WT and D80 F54L to HA suggest that F54 in D80 does not have a critical role in HA binding and rather binding is mainly mediated through CDR-H3 Y98 (Avnir et al., 2014). This observation is also in agreement with the study by Pappas et al. (2014) that somatic mutations in the VH-segment of HV1-69-sBnAbs can compensate for the critical role of F54 in HA binding.

In addition, substitutions at position 58 are detrimental to G6 binding, however, all the HV1-69-sBnAbs defined by substitutions at position 58 (Figure 1) are still able to bind HA (except of F10, discussed below). In the available crystal structure of F10 bound to HA, the germline-encoded residue of N58 is located on a beta strand following CDR-H2 and does not make any hydrogen bonds or vdW contacts with HA (Sui et al., 2009). Aligning the D80 Fab structure onto F10, N58 is located

F94 (VL) and W33 (VH) (Figure 5D). The VL of D80 also makes one hydrogen bond from R96 to hG6.3 Q90 (Table S2). Taken together, analysis of vdW, hydrogen bonding, and pi-stacking interactions identify D80 residues that contribute to intermolecular interactions with the G6 as CDR-H1 positions 31 and 33, CDR-H2 positions 53–58, and CDR-H3 positions 97–99, with the key positions of the idiotope located on CDR-H2.

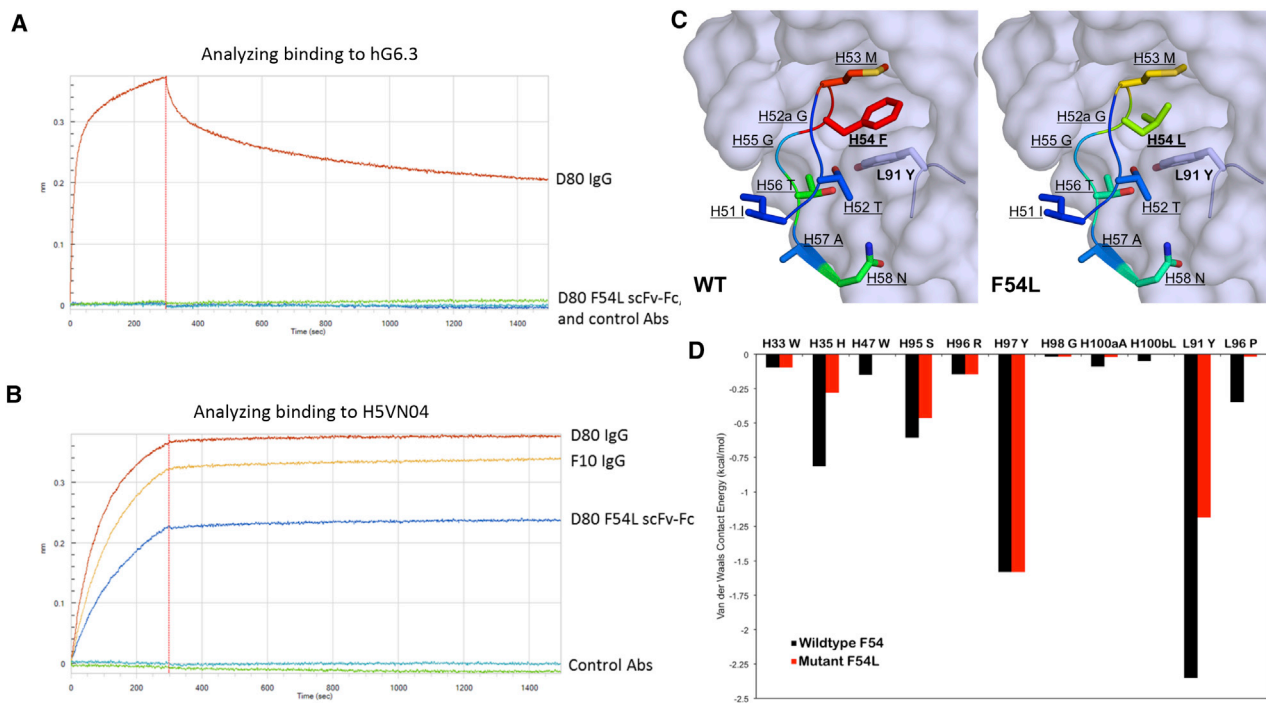### Comparison of D80 Unbound and hG6.3-Bound Structures

The overall unbound versus hG6.3-bound D80 structures do not have any major backbone changes except a slight increase in the angle between the VH and CH1 domains relative to each other (1°–3°, Figures S2A–S2C), which may also be affected by crystal packing, suggesting a lock-and-key type protein-protein binding. To compare the bound and unbound structures quantitatively, the distance difference matrix was calculated for the heavy chain of D80 Fab fragment (Figures S2D–S2F; Supplemental Experimental Procedures). In accordance with the increase in inter-domain angle, the majority of distance changes correspond to increase in distance between residues in D80's VH and CH1 domains when bound to hG6.3. Within each domain the changes were much more subtle, with the most considerable changes in the CDR-H1 loop and a few residues displaying distance changes of more than 2 Å in CDR-H2 and CDR-H3 loops. The pi-stacking interaction network described above (Figure 5D) is conserved between the unbound and bound structures of D80 and may contribute to stabilizing the loop structures in a binding-competent state in the unbound form. Overall, the similarity of CDR loops regardless of whether D80 is bound to hG6.3 or not indicates that the epitope pre-exists in the unbound state and

Figure 6. Changing D80 F54L Abolished Binding to hG6.3 but Maintained Binding to H5VN04

(A) A D80 variant in which the CDR-H2 Phe54 was substituted with Leu54 (D80 F54L) did not show any binding activity to hG6.3 as analyzed by using an Octet RED96 instrument.

(B) This variant, however, did retain strong binding activity against the H5VN04 HA.

(C and D) Focused view on D80 CDR-H2 colored blue to red for increasing vdW contact energy with hG6.3, containing Phe54 (left, red) in the crystal structure and modeled Leu54 (right, yellow) (C), indicating that the vdW contacts would decrease with F54L substitution, primarily with (D) L91 Y and H35 H of hG6.3, and amount to an overall reduction in vdW contact energy of 5 kcal/mol.

in the same position in D80 with respect to HA and hence is not involved in any intermolecular interactions (Figure 4B). Thus, the difference in the epitope used by D80 in hG6.3 versus HA binding explains why HV1-69-sBnAbs with a substitution at N58 can retain HA binding despite becoming G6-unreactive.

Establishing Specificity of G6 Binding to _IGHV1-69_ F-Alleles through scFv-Phagemid Library Panning

The breadth of G6 reactivity for rearranged _IGHV1-69_ genes was further investigated. An assay was developed in which our 27 billion-member Mehta I/II non-immune human Ab scFv-phagemid-Ab library was panned against beads coupled with G6 (Figure 7). DNA sequences from the phagemid-Abs recovered from the beads confirmed that G6 is highly specific to _IGHV1-69_ F-allele group Abs (Figure 7A). Long-read PacBio next generation sequencing of the pre-selected phagemid-Ab library confirmed the G6-selected _IGHV1-69_ F-allele-encoded Abs was not due to the biased Mehta I/II library composition or due to absence of _IGHV1-69_ L-alleles (not shown). High diversity in the eluted Abs was observed with respect to D-segments (Figure 7B), J-segments (Figure 7C), and CDR-H3 length (Figure 7E). Promiscuous use of kappa and lambda light chains was also noted (Figure 7D). A single noticeable difference in the D-segment usage between the G6-selected and unselected Abs is that the former had only one Ab comprised of the IGHD2-15*01 D-segment, which does

not encode CDR-H3 Tyr's in any reading frame, versus ~8% in the unselected Abs (Figure S3A).

V-segment analysis revealed preferential binding to non-mutated V-segments (Figures 7F and S4). Our analyses reveal a paucity of CDR-H2 amino acid substitutions (Figure 7G): explicitly, of the 142 _IGHV1-69*01_ Abs, only 13 Abs had amino acid substitutions in the CDR-H2 domain, while 36 Abs had amino acid substitutions in the CDR-H1 domain (Figure S4). This biased distribution of CDR-H1 versus CDR-H2 substitutions is in line with the importance of germline CDR-H2 residues mentioned above. In addition, none of the CDR-H2 substitutions involved changes in F54, while analysis of CDR-H2 amino acid sequences of 75 _IGHV1-69_ hv1263 allele-encoded Abs in the pre-selected library showed that 8 had L54F substitutions, and of these, none exhibited complete reversal to the F-allele 51p1 CDR-H2 sequence IIPIFGTA, thereby further demonstrating the unlikelihood of G6 binding to hv1263 allele-encoded Abs (Figure S3B).

G6 and hG6.3 Favor Binding to Antibodies Defined by Non-mutated _IGHV1-69_ V- Segments

A subset of G6-reactive phagemid-Abs from the panning assays with a range of V-segment mutations was chosen and analyzed for their binding against both G6 and hG6.3 by ELISA assay that utilized the Meso Scale Discovery (MSD) technology. The MSD
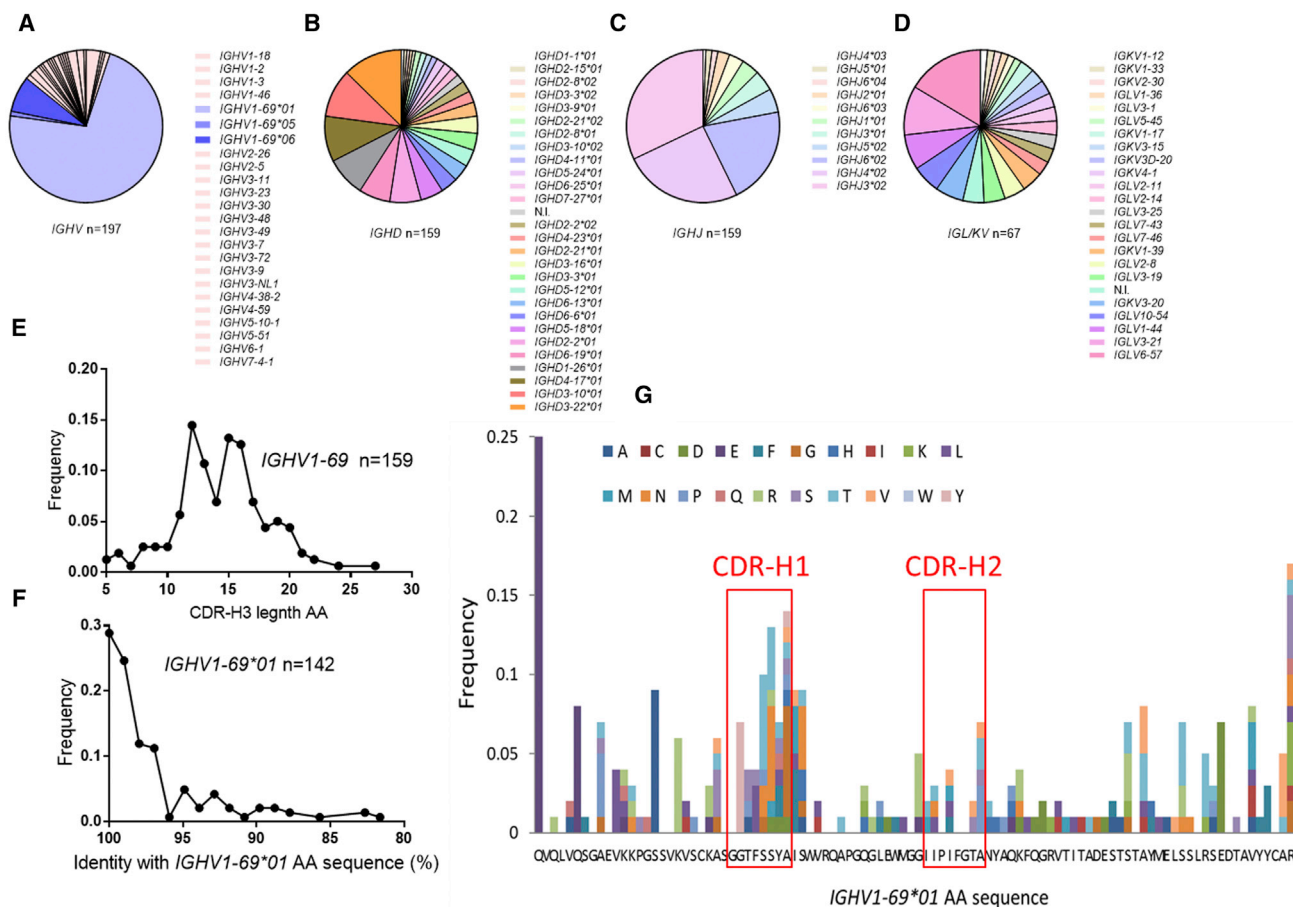
Figure 7. Panning a Non-immune Human scFv Phagemid-Ab Library against G6

Human scFv phagemid-Ab display library was mixed with beads coupled with G6. After phagemid elution and bacterial infection, colonies were sequenced and immunogenetic analysis was carried out.

(A–E) Each individual sequence represents one phagemid-Ab. (A) Of 197 sequences containing functional VH genes, 81% were composed of *IGHV1-69* germline gene and all *IGHV1-69* sequences belonged to the F-allele group. Further analysis of the *IGHV1-69* dataset points to high diversity in (B) D-segments, (C) J-segment, (D) type of light chain, and in (E) CDR-H3 length.

(F) In contrast, analyzing the frequency of V-segment amino acids changes for the 142 *IGHV1-69*01* Ab-sequences showed that G6 preferentially binds to Abs characterized by non-mutated V-segments.

(G) The amino acid substitution diversity in the 142 *IGHV1-69*01* Ab-sequences.

signal obtained from four dilution points was used to calculate area under the curve (AUC) values and these were tabulated in Figure S5A. The majority of the *IGHV1-69* phagemid-Abs (17 of 19) were defined by AUC values that were within or above one SD of the mean (mean ± 1 SD = G6 8.91E + 05 ± 3.55E + 05; hG6.3 6.80E + 05 ± 2.83E + 05). However, two Abs (S60 and F66) encoding a germline CDR-H2 region had lower AUC values than the mean minus one SD. Although, they did have 8 and 2 substitutions, respectively, in their V-segments inspection of these two Abs against the panel of Abs that showed stronger hG6.3 binding did not reveal an obvious cause for the weaker binding (Figure S5B). In agreement with our previous report on humanization of G6 (Chang et al., 2016), D80 had weaker binding activity against G6 and hG6.3 as defined by the AUC values of 1.67E + 05 and 7.83E + 04, respectively, and the three non-*IGHV1-69* phagemid-Abs exhibited only background binding

activities that were defined by an average AUC of G6, mean ± 1 SD = 3.68E + 03 ± 2.50 + 03; hG6.3, 2.69E + 03 ± 2.12E + 03. From these studies, we conclude that G6 shows preferential binding for the germline CDR-H2 loop, and with a few exceptions, does not show major differences between the *IGHV1-69* F-allele Abs despite variability in V-segment amino acid substitutions, CDR-H3 composition, and type of light chain.

The Binding Conformation of *IGHV1-69* Abs with Non-mutated V-Segment against hG6.3 Based on the D80 Crystal Structure

The D80-hG6.3 structure was then used to model the binding of *IGHV1-69* Abs comprised of non-mutated V-segments. Two 51p1 *IGHV1-69* Abs with germline V-segments and available unbound crystal structures, 1-69/B3 (Teplyakov et al., 2016), and 3B4 (Tu et al., 2016), were expressed as scFv-phagemid Abs

and were found to bind G6/hG6.3 stronger than D80 in MSD ELISA assay (data not shown). The unbound structures were aligned onto the D80 in the complex, followed by energy minimization (see the Experimental Procedures). The CDR-H2 in the resulting G6-bound structures of both Abs superimpose very well with D80 (Figure S6). Most importantly, 1-69/B3 and 3B4 are able to maintain the critical interactions of F54 and N58 in CDR-H2 (Figures S6C and S6D). However, 3B4 and 1-69/B3 have more extensive contacts with hG6.3 compared to D80, resulting in more buried solvent accessible surface area upon binding (1,400 $Å^2$; more than 50% compared to D80) and a corresponding more than 50% increase in the intermolecular vdW interaction energy. This increase is due to enhanced intermolecular interactions of CDR-H3 as well as with VL, suggesting that while the conformation of CDR-H2 is critical to G6 binding, further interactions including those with CDR-H3 and the light chain can enhance the binding strength of G6-reactive Abs.

HV1-69-sBnAb F10 Is G6-Unreactive Due to Prolines in CDR-H2

Finally, to understand why HV1-69-sBnAb F10 is G6-unreactive despite retaining the germline N58, binding of F10 to hG6.3 was modeled using the D80-hG6.3 crystal structure as a template (Figure 4C). When F10's CDR-H2 is aligned onto the D80 structure to maintain the critical van der Waals contacts of the F54 side chain, N58 is positioned too far away from hG6.3 to maintain any of its three intermolecular hydrogen bonds (Figure 4; Table S2). This displacement relative to the same position in D80 is due to a kink in the beta strand following CDR-H2 caused by a proline substitution at position 57 preceding N58. Thus, the proline substitution at position 57 rigidifies CDR-H2 and creates a kink in the backbone structure that renders F10 unable to simultaneously establish the key F54 and N58 interactions. In accordance, none of the HV1-69-sBnAb with an A57P substitution in our initial panel was G6 reactive (Figure 1B). However, mutation of position 57 back to Ala in F10 was not sufficient to restore G6 reactivity (data not shown), most likely due to an I53M substitution next to a second proline in CDR-H2, the germline P52a. The M53 side chain has a different conformation in F10 compared to D80 and can be accommodated at the binding interface only in the presence of a neighboring P52aG substitution that allows backbone flexibility, as is the case in D80. Thus, G6 binding can be lost in multiple ways, including due to a substitution of the critical germline N58 itself, or a proline substitution at the preceding A57 that causes N58 to lose intermolecular interactions.

DISCUSSION

The anti-Id+ *IGHV1-69* Ab G6 has been used extensively for over 30 years to characterize biologically important antibody processes in humans. Since G6's discovery, recognition of important functions of IGHV polymorphism and related biased germline gene usage in wellness and disease has grown, yet there is a paucity of well-characterized anti-Id+ reagents that can be used to monitor these serologic responses. In this study, an in-depth investigation was conducted into the binding epitope of the humanized version of G6, hG6.3 (Chang et al., 2016). We solved the crystal structures of hG6.3 in complex with anti-influ-

enza HV1-69-sBnAb D80, and D80 alone (Figure 3). The hG6.3 idiotope is centered around the CDR-H2 loop of D80, with the M53 and F54 at the tip of this loop inserting into a pocket in hG6.3, and the core of the idiotope extending to N58 (Figures 4 and 5) and interacting with both the heavy and light chains of hG6.3 (Figure S7). G6 prefers binding to Abs for which CDR-H2 is in the germline configuration (Figures 7, S4, and S5). The anti-Id tolerates hydrophobic amino acid substitutions at position I53 (Figure S4); however, in striking contrast, the critical role of germline F54 for binding is absolute. The germline CDR-H2 boundary residue N58 (Figure 4), which participates in an intermolecular hydrogen bonding network, also greatly contributes to the binding energy. Maintaining the interactions of both F54 and N58 simultaneously is required for binding G6 but not for HA binding where only the former is necessary. The G6 idiotope also appears to require germline G55 as other side chains would sterically clash with Tyr91 (Figures 1B, S4, and S7B); however, this position is not invariant for HV1-69-sBnAbs (Avnir et al., 2014). Small amino acid side chain substitutions of T56V, T56A, and T56S are rarely found but larger side chains are not seen and would be predicted to clash with hG6.3 light chain residues (Figures S4 and S7). We conclude that the hG6.3 angle of approach to the main core of the idiotope, which is a continuous string of CDR-H2 residues starting with M53 and ending with N58 is such that hG6.3 provides a hydrophobic pocket lined between the heavy and light chains where M53 and F54 side chains are inserted, whereas the hG6.3 light chain provides polar side chains (N32, S92, Q93) that form hydrogen bonds to T56 and N58.

The binding interaction observed between hG6.3 and D80, in which the D80 idiotope is not centered on the axis of the β-barrel formed by the β strands of the VH and VL domains, is unusual but not unprecedented. Co-crystallographic studies of human IgM RF-AN bound to IgG4 Fc showed that the Ab residues involved in autorecognition are all located at the edge of the conventional combining site surface, leaving much of the RF light chain CDRs (CDR-L1, -L2, and -L3) potentially available for recognition of a different antigen (Corper et al., 1997). hG6.3 binding to D80 results in the hG6.3 heavy chain covering the apex of the D80 heavy chain and the hG6.3 light chain is positioned in front of the D80 heavy chain-light chain interface. This topography of interaction results in the notable lack of any contribution from D80 CDR-L1 and -L2 to hG6.3 binding (Figure 3C). Whether this remaining D80 VL surface area could be available for binding another antigen is unknown but would require a narrow angle of approach that does not rely on the main CDR loops of D80. Because D80 utilizes the *IGKV3-20* light chain germline gene, this could be tested experimentally with anti-*IGKV3-20* idiotypic Abs or antigens that show biased binding of this light chain (de Re et al., 2009). A similar hypothesis could be made for any of the Id+ *IGHV1-69* Abs that are recognized by G6.

The results from the G6 panning studies (Figure 7) demonstrate the remarkable breadth of binding to the family of 51p1 *IGHV1-69* Abs. The hG6.3:D80 co-crystal structure shows that the pocket in hG6.3 is not entirely filled by D80, but could play a role in the diversity of antibody binding (Figure S1). A wide variety of CDR-H3 compositions with varying length and amino acid substitutions are tolerated (Figures 7 and S4). The crystal

structure demonstrates that hG6.3 primarily makes contact with the D80 heavy chain, which is in agreement with the broad range of light chain pairing that is seen from our G6 panning studies. Soluble VH1-69/F10 VH domains also bind G6 with even higher affinity than VH1-69/F10 scFvs that may be due to an increase in buried surface area and contacts with CDR-H3 (Figure 3B and data not shown). Many CDR-H1 substitutions appear to be well-tolerated, as are substitutions in FR1-3 and CDR-H4 (Avnir et al., 2014; Sela-Culang et al., 2013) in contrast to the paucity of CDR-H2 amino acid substitutions that forms the core of the G6 idiotope (Figure S4). In agreement with the lack of G6 binding to hv1263 encoding *IGHV1-69* Abs, modeling of L54 in the hG6.3/D80 complex structure suggests substantial losses in vdW contact likely destabilizes the intermolecular interface with hG6.3 (Figure 6). Thus, the highly specific yet broad range of binding activities of G6 represents a unique property that has not been described for other anti-Id⁺ Abs.

We further defined the structural features of the 51p1 alleles that would lead to a loss of the G6 idiotope but retention of HA binding and vice versa. The HV1-69-sBnAb family is defined, at least in part, by critical amino acid substitutions in the VH segment including germline CDR-H2 ($II_{52}P_{52a}I_{53}F_{54}GTA$) at positions I52 or P52a together with triad of a hydrophobic amino acid at position 53, Phe54, and properly positioned CDR-H3 Tyr (Avnir et al., 2014). The majority of tested HV1-69-sBnAbs did not bind to G6 despite the fact that all were comprised of the *IGHV1-69* 51p1 group (Figure 1A) and encode CDR-H2 F54 (Potter et al., 1999). The three G6-reactive HV1-69 sBnAbs had the common features of P52aA/G substitutions, I53V/M hydrophobic substitutions, and a triplet of CDR-H3 Tyrs (Avnir et al., 2014). The triple tyrosine motif in D80 is involved in an extensive pi-stacking interaction network that may pre-organize the binding epitope and promote tight binding to G6 and HA (Figure 5); related tyrosine pi-stacking interactions may also be involved in 70-1F02 and CR6331 binding to both G6 and HA. Interestingly, the chimeric VH1-69/F10 CDR-H2 I52S and I53M variants bind with decreased affinity with respect to G6 compared to VH1-69/F10 (Figure 2B), while the VH1-69/F10 CDR-H2 I52S variant is capable of binding to HA, but VH1-69/F10 and VH1-69/F10 CDR-H2 I53M do not (Avnir et al., 2014). The flexible CDR-H2 residues introduced by the P52aA/G substitutions together with germline A57 may increase CDR-H2 loop flexibility and are features of the G6 Id⁺ HV1-69-sBnAbs whereas many of the G6 non-reactive HV1-69-sBnAbs contain proline at these positions. G6 binding can be lost in multiple ways, including due to a substitution of the critical germline N58 itself, or a proline substitution at the preceding A57 that causes N58 to lose intermolecular interactions. These results suggest HV1-69-sBnAbs are highly sensitive to structural variation around the core F54 contact residue that appear to greatly affect the conformation of the CDR-H2 loop with respect to optimal binding for HA and G6 idiotope expression.

In conclusion, the growing recognition that IGHV polymorphism and biased VH germline gene usage are important, albeit understudied, features of the Ab response in health and disease is reshaping our thinking on how this knowledge can be applied to precision medicine. In the area of host defense, hG6.3 could be used to monitor the loss of G6 CRI in the circulating *IGHV1-69* Ab pool as B cells evolve to become memory B cells and HV1-69-sBnAbs secreting plasma cells in response to seasonal (Corti et al., 2010) and emerging HA-stem derived "universal" influenza vaccines (Krammer, 2015). The G6 CRI may also be useful for monitoring B cells and Abs that bind to and neutralize HCV and MERS-CoV, respectively (Chan et al., 2001; Tang et al., 2014; Ying et al., 2015). In the emerging field of oncoimmunology, the high presence of G6 CRI on unmutated BCRs seen in *IGVH1-69*-encoded B-CLL (Chang et al., 2016; Hamblin et al., 1999), and the recognition of other *IGHV1-69* disorders involving pathophysiologic B cell expansions (Chan et al., 2001; Miklos et al., 2000) could provide an avenue of therapeutic intervention through hG6.3-mediated immune clearance. In addition, hG6.3-based idiotype mapping (Idio-Seq) could add an important new dimension to the field of immune recognition where advances in the high-throughput sequencing and analysis of expressed Ab repertoires (BCR-seq) in peripheral blood B cells and LC-MS/MS proteomic spectrotyping of antigen-specific Abs (IG-seq) allow us to characterize, with unparalleled accuracy, the serological repertoire to each of the Ab components (Lee et al., 2016). This knowledge will aid in our understanding of how the serological repertoire changes in response to vaccination, infection, cancer, and auto-immune diseases. Defining the expressed G6 CRI repertoire and understanding how Abs encoding a *IGHV1-69* VH segment germline configuration participate in wellness and pathologic humoral responses (Watson et al., 2017) could be important part of this ongoing paradigm shift.

EXPERIMENTAL PROCEDURES

Sequence Analysis of Abs

Abs were numbered according to the Kabat numbering scheme. CDR-H1, H2 are defined according to IMGT's definitions. For CDR-H3, residues are shown from Cys92 to Trp103 and for CDR-H3/J residues are shown from Cys92 to Ser113. CDR-H4 was defined based on our previous study (Avnir et al., 2014). Ab sequences were analyzed by using either IgBlast (Ye et al., 2013) or IMGT/HighV-QUEST (Alamyar et al., 2012).

Construction and Expression of HV1-69-sBnAbs Variants

The HV1-69-sBnAbs variants were constructed and expressed as scFv as described in Avnir et al. (2014). The original (WT) CDR-H3s and light chains were maintained in all analyzed HV1-69-sBnAbs variants.

Binding Assays of HV1-69-sBnAbs to G6 and hG6.3

For Abs F10, A66, G17, D7, D8 and H40, standard ELISA assay was performed by coating MaxiSorp plates with G6, adding HV1-69-sBnAbs in the scFv-Fc format, and detecting bound HV1-69-sBnAbs with anti-human Fc conjugated with HRP. For the IgG Abs 1009-3E06, 1009-3B05, 70-5B03, and 70-1F02 (Wrammert et al., 2011) and for scFvs CR6331 and CR6261 (Throsby et al., 2008) a Biacore T100 instrument was used in which the Abs were flowed over a CM5 chip that was immobilized with an anti-mouse-Ab and captured G6. For C9114 scFv-Fc an Octet RED96 instrument was used in which biotinylated-hG6.3 was captured on streptavidin sensor after which the sensor was moved to a well containing the scFv-Fc CR9114 Ab.

Binding Kinetics Assay of HV1-69-sBnAb Germline Variants

Biacore T100 single cycle kinetics assays were performed for VH1-69/F10, VH1-69/A66, and VH1-69/CR6261 scFvs by using a CM5 chip that was immobilized with an anti-mouse-Ab and captured G6 at a level of ~320 response units (RUs). Similarly, the various VH1-69/F10 variants were

analyzed for G6 binding when each variant was used at a single concentration of 2.85 μg/mL.

B Cell Receptor Cross Linking Assay

The heavy chain and light chains of the various VH1-69/F10 variants were cloned into a B cell receptor vector and the B cell cross linking assays with G6 or hG6.3 were executed as described previously (Hoot et al., 2013) and as detailed in the Figure 2 legend.

Protein Expression, Purification, and Crystallization

For crystallographic purposes, Fab fragments were expressed in insect cells using a baculovirus expression system. Fab fragments were purified using a polyhistidine tag with nickel-affinity chromatography and subsequent size exclusion chromatography. For unbound D80 crystallization, the D80 Fab fragment crystals were grown at 20°C by hanging-drop vapor diffusion in a solution using 20% PEG 4000, 0.2 M $CaCl_2$, and 0.1 M Tris pH 8.4. D80 crystallized in a $P\ 2_12_12_1$ space group with 2 molecules in the asymmetric unit and unit cell dimensions of a = 89.0, b = 91.6, and c = 106.8 Å. For D80-G6 complex crystallization, the D80-G6 Fab fragment complex crystals were grown at 20°C by hanging-drop vapor diffusion in a solution using 0.1 M NH_4SO_4 and 12% PEG 3350. The D80-G6 complex was crystallized in a C 1 2 1 space group with 1 molecule in the asymmetric unit and unit cell dimensions of a = 143.2, b = 50.8, and c = 139.7 Å.

Diffraction Data Collection and Structure Solution

Diffraction data was collected at cryogenic temperatures using synchrotron radiation at the GM/CA-CAT 23-ID-B beam line at the Argonne National Laboratory (Advanced Photon Source, Chicago, IL). Data was indexed and scaled using xia2 and HKL3000 (Collaborative Computational Project, Number 4, 1994; Kabsch, 2010; Minor et al., 2006; Winter et al., 2013). Molecular replacement solutions were determined using M-RAGE in PHENIX (Adams et al., 2010; Bunkóczi et al., 2013). Cycles of rigid body, restrained, and TLS refinement with subsequent model building were performed using phenix.refine in PHENIX and Coot, respectively (Adams et al., 2010; Emsley et al., 2010).

Binding Assays of the D80 F54L Variant

Mutagenesis of D80 F54 scFv-Fc to D80 L54 scFv-Fc was achieved using QuikChange Lightning kit according to manufacturer's protocol. Binding assays were performed using the Octet RED96 instrument with streptavidin sensors. Biotinylated hG6.3 or biotinylated hemagglutinin H5VN04 (H5 A/VietNam/1203/04) were loaded at a concentration of 0.5 μg/mL, and the various analyzed Abs were used at a concentration of 10 μg/mL.

Panning the Naive Human scFv Phagemid Library against Beads Coupled with G6

Magnetic M-280 Tosylactivated DynaBeads were coupled with an isotype control mouse Ab and with G6 according to the manufacturer's protocol. The Mehta I/II phagemid library mixture was subtracted of non-specific and mouse-IgG binders by performing two rounds of subtractions with the isotype control beads after which the phagemid suspension was added to G6 coupled beads. Following six washes with TBS-Tween-20, the phagemids were eluted with 100 mM of TEA and neutralized with PBS. The eluted phagemid suspension was used to infect TG1 cells from which single clones were sequenced. The results of Figures 7 and S4 were obtained from several G6 panning assays.

DATA AND SOFTWARE AVAILABILITY

The accession numbers for the atomic coordinates for the crystal structures of D80 Fab and D80 Fab bound to hG6.3 Fab reported in this paper are PDB: 5JQD and 5JO4.

SUPPLEMENTAL INFORMATION

Supplemental Information includes Supplemental Experimental Procedures, seven figures, and two tables and can be found with this article online at https://doi.org/10.1016/j.celrep.2017.11.056.

AUTHOR CONTRIBUTIONS

Y.A. conceived project, mutagenesis, phage display, and binding kinetics studies, molecular modeling, and wrote the manuscript. K.L.P. performed the crystallization, data collection, structure determination and analysis, and wrote the manuscript. Z.Z. performed crystallization, data collection, and structure determination. B.J.H. and M.-F.B. performed the data collection for structure determination. S.H. performed the structural analysis and molecular modeling. H.Z. and E.C.P. performed the phage display studies. J.S. performed the ELISA assay and humanization of hG6.3. V.B.K. performed the humanization of hG6.3 and the biological studies. M.G. and R.J. performed the humanization of hG6.3. A.T.M. and L.S. performed the BCR studies. T.F.K. and J.D.J. designed the research and obtained funding. J.P.W. and R.W.F designed the research, obtained funding, and edited the manuscript. Q.Z. co-supervised the humanization, mutagenesis, and phage display studies. N.K.Y. co-supervised crystallographic, structural analysis, and molecular modeling studies, designed the research, and wrote and edited the manuscript. C.A.S. co-supervised crystallographic, structural analysis, and molecular modeling studies, wrote the manuscript, designed the research, and obtained funding. W.A.M. conceived the project, co-supervised humanization, mutagenesis, phage display, and molecular modeling studies, wrote and edited the manuscript, designed the research, and obtained funding.

DECLARATION OF INTERESTS

W.A.M. has a financial interest in AR Pharma, the licensee of hG6.3. The content of this manuscript is solely the responsibility of the authors and does not necessarily represent the official views of the NIH or Department of Defense.

REFERENCES

Adams, P.D., Afonine, P.V., Bunkóczi, G., Chen, V.B., Davis, I.W., Echols, N., Headd, J.J., Hung, L.W., Kapral, G.J., Grosse-Kunstleve, R.W., et al. (2010). PHENIX: a comprehensive Python-based system for macromolecular structure solution. Acta Crystallogr. D Biol. Crystallogr. 66, 213–221.

Alamyar, E., Duroux, P., Lefranc, M.P., and Giudicelli, V. (2012). IMGT(®) tools for the nucleotide analysis of immunoglobulin (IG) and T cell receptor (TR) V-(D)-J repertoires, polymorphisms, and IG mutations: IMGT/V-QUEST and IMGT/HighV-QUEST for NGS. Methods Mol. Biol. 882, 569–604.

Avnir, Y., Tallarico, A.S., Zhu, Q., Bennett, A.S., Connelly, G., Sheehan, J., Sui, J., Fahmy, A., Huang, C.Y., Cadwell, G., et al. (2014). Molecular signatures of hemagglutinin stem-directed heterosubtypic human neutralizing antibodies against influenza A viruses. PLoS Pathog. 10, e1004103.

Avnir, Y., Watson, C.T., Glanville, J., Peterson, E.C., Tallarico, A.S., Bennett, A.S., Qin, K., Fu, Y., Huang, C.Y., Beigel, J.H., et al. (2016). IGHV1-69 polymorphism modulates anti-influenza antibody repertoires, correlates with IGHV utilization shifts and varies by ethnicity. Sci. Rep. 6, 20842.

OPEN
ACCESS
CellPress

Bunkóczi, G., Echols, N., McCoy, A.J., Oeffner, R.D., Adams, P.D., and Read, R.J. (2013). Phaser.MRage: automated molecular replacement. Acta Crystallogr. D Biol. Crystallogr. *69*, 2276–2286.

Cerutti, A., Cols, M., and Puga, I. (2013). Marginal zone B cells: virtues of innate-like antibody-producing lymphocytes. Nat. Rev. Immunol. *13*, 118–132.

Chan, C.H., Hadlock, K.G., Foung, S.K., and Levy, S. (2001). V(H)1-69 gene is preferentially used by hepatitis C virus-associated B cell lymphomas and by normal B cells responding to the E2 viral antigen. Blood *97*, 1023–1026.

Chang, D.K., Kurella, V.B., Biswas, S., Avnir, Y., Sui, J., Wang, X., Sun, J., Wang, Y., Panditrao, M., Peterson, E., et al. (2016). Humanized mouse G6 anti-idiotypic monoclonal antibody has therapeutic potential against IGHV1-69 germline gene-based B-CLL. MAbs *8*, 787–798.

Charles, E.D., Orloff, M.I., Nishiuchi, E., Marukian, S., Rice, C.M., and Dustin, L.B. (2013). Somatic hypermutations confer rheumatoid factor activity in hepatitis C virus-associated mixed cryoglobulinemia. Arthritis Rheum. *65*, 2430–2440.

Collaborative Computational Project, Number 4 (1994). The CCP4 suite: programs for protein crystallography. Acta Crystallogr. D Biol. Crystallogr. *50*, 760–763.

Corper, A.L., Sohi, M.K., Bonagura, V.R., Steinitz, M., Jefferis, R., Feinstein, A., Beale, D., Taussig, M.J., and Sutton, B.J. (1997). Structure of human IgM rheumatoid factor Fab bound to its autoantigen IgG Fc reveals a novel topology of antibody-antigen interaction. Nat. Struct. Biol. *4*, 374–381.

Corti, D., Suguitan, A.L., Jr., Pinna, D., Silacci, C., Fernandez-Rodriguez, B.M., Vanzetta, F., Santos, C., Luke, C.J., Torres-Velez, F.J., Temperton, N.J., et al. (2010). Heterosubtypic neutralizing antibodies are produced by individuals immunized with a seasonal influenza vaccine. J. Clin. Invest. *120*, 1663–1673.

Corti, D., Cameroni, E., Guarino, B., Kallewaard, N.L., Zhu, Q., and Lanzavecchia, A. (2017). Tackling influenza with broadly neutralizing antibodies. Curr. Opin. Virol. *24*, 60–69.

Damle, R.N., Wasil, T., Fais, F., Ghiotto, F., Valetto, A., Allen, S.L., Buchbinder, A., Budman, D., Dittmar, K., Kolitz, J., et al. (1999). Ig V gene mutation status and CD38 expression as novel prognostic indicators in chronic lymphocytic leukemia. Blood *94*, 1840–1847.

de Re, V., Simula, M.P., Pavan, A., Garziera, M., Marin, D., Dolcetti, R., de Vita, S., Sansonno, D., Geremia, S., and Toffoli, G. (2009). Characterization of antibodies directed against the immunoglobulin light kappa chain variable chain region (VK) of hepatitis C virus-related type-II mixed cryoglobulinemia and B-cell proliferations. Ann. N Y Acad. Sci. *1173*, 152–160.

Dreyfus, C., Laursen, N.S., Kwaks, T., Zuijdgeest, D., Khayat, R., Ekiert, D.C., Lee, J.H., Metlagel, Z., Bujny, M.V., Jongeneelen, M., et al. (2012). Highly conserved protective epitopes on influenza B viruses. Science *337*, 1343–1348.

Durrant, J.D., Votapka, L., Sørensen, J., and Amaro, R.E. (2014). POVME 2.0: an enhanced tool for determining pocket shape and volume characteristics. J. Chem. Theory Comput. *10*, 5047–5056.

Ekiert, D.C., Bhabha, G., Elsliger, M.A., Friesen, R.H., Jongeneelen, M., Throsby, M., Goudsmit, J., and Wilson, I.A. (2009). Antibody recognition of a highly conserved influenza virus epitope. Science *324*, 246–251.

Emsley, P., Lohkamp, B., Scott, W.G., and Cowtan, K. (2010). Features and development of Coot. Acta Crystallogr. D Biol. Crystallogr. *66*, 486–501.

Fais, F., Ghiotto, F., Hashimoto, S., Sellars, B., Valetto, A., Allen, S.L., Schulman, P., Vinciguerra, V.P., Rai, K., Rassenti, L.Z., et al. (1998). Chronic lymphocytic leukemia B cells express restricted sets of mutated and unmutated antigen receptors. J. Clin. Invest. *102*, 1515–1525.

Grey, H.M., Mannik, M., and Kunkel, H.G. (1965). Individual antigenic specificity of myeloma proteins. characteristics and localization to subunits. J. Exp. Med. *121*, 561–575.

Hamblin, T.J., Davis, Z., Gardiner, A., Oscier, D.G., and Stevenson, F.K. (1999). Unmutated Ig V(H) genes are associated with a more aggressive form of chronic lymphocytic leukemia. Blood *94*, 1848–1854.

Hashimoto, S., Dono, M., Wakai, M., Allen, S.L., Lichtman, S.M., Schulman, P., Vinciguerra, V.P., Ferrarini, M., Silver, J., and Chiorazzi, N. (1995). Somatic diversification and selection of immunoglobulin heavy and light chain variable region genes in IgG+ CD5+ chronic lymphocytic leukemia B cells. J. Exp. Med. *181*, 1507–1517.

Hoot, S., McGuire, A.T., Cohen, K.W., Strong, R.K., Hangartner, L., Klein, F., Diskin, R., Scheid, J.F., Sather, D.N., Burton, D.R., and Stamatatos, L. (2013). Recombinant HIV envelope proteins fail to engage germline versions of anti-CD4bs bNAbs. PLoS Pathog. *9*, e1003106.

Johnson, T.A., Rassenti, L.Z., and Kipps, T.J. (1997). Ig VH1 genes expressed in B cell chronic lymphocytic leukemia exhibit distinctive molecular features. J. Immunol. *158*, 235–246.

Kabsch, W. (2010). XDS. Acta Crystallogr. D Biol. Crystallogr. *66*, 125–132.

Keating, M.J., Chiorazzi, N., Messmer, B., Damle, R.N., Allen, S.L., Rai, K.R., Ferrarini, M., and Kipps, T.J. (2003). Biology and treatment of chronic lymphocytic leukemia. Hematology Am. Soc. Hematol. Educ. Program *2003*, 153–175.

Kipps, T.J., Tomhave, E., Pratt, L.F., Duffy, S., Chen, P.P., and Carson, D.A. (1989). Developmentally restricted immunoglobulin heavy chain variable region gene expressed at high frequency in chronic lymphocytic leukemia. Proc. Natl. Acad. Sci. USA *86*, 5913–5917.

Krammer, F. (2015). The quest for a universal flu vaccine: Headless HA 2.0. Cell Host Microbe *18*, 395–397.

Kunkel, H.G., Mannik, M., and Williams, R.C. (1963). Individual antigenic specificity of isolated antibodies. Science *140*, 1218–1219.

Lee, J., Boutz, D.R., Chromikova, V., Joyce, M.G., Vollmers, C., Leung, K., Horton, A.P., DeKosky, B.J., Lee, C.H., Lavinder, J.J., et al. (2016). Molecular-level analysis of the serum antibody repertoire in young adults before and after seasonal influenza vaccination. Nat. Med. *22*, 1456–1464.

Mageed, R.A., Dearlove, M., Goodall, D.M., and Jefferis, R. (1986). Immunogenic and antigenic epitopes of immunoglobulins. XVII–Monoclonal antibodies reactive with common and restricted idiotopes to the heavy chain of human rheumatoid factors. Rheumatol. Int. *6*, 179–183.

Miklos, J.A., Swerdlow, S.H., and Bahler, D.W. (2000). Salivary gland mucosa-associated lymphoid tissue lymphoma immunoglobulin V(H) genes show frequent use of V1-69 with distinctive CDR3 features. Blood *95*, 3878–3884.

Minor, W., Cymborowski, M., Otwinowski, Z., and Chruszcz, M. (2006). HKL-3000: the integration of data reduction and structure solution–from diffraction images to an initial model in minutes. Acta Crystallogr. D Biol. Crystallogr. *62*, 859–866.

Newkirk, M.M., Mageed, R.A., Jefferis, R., Chen, P.P., and Capra, J.D. (1987). Complete amino acid sequences of variable regions of two human IgM rheumatoid factors, BOR and KAS of the Wa idiotypic family, reveal restricted use of heavy and light chain variable and joining region gene segments. J. Exp. Med. *166*, 550–564.

Oudin, J., and Michel, M. (1969a). Idiotypy of rabbit antibodies. I. Comparison of idiotypy of antibodies against Salmonella typhi with that of antibodies against other bacteria in the same rabbits, or of antibodies against Salmonella typhi in various rabbits. J. Exp. Med. *130*, 595–617.

Oudin, J., and Michel, M. (1969b). Idiotypy of rabbit antibodies. II. Comparison of idiotypy of various kinds of antibodies formed in the same rabbits against Salmonella typhi. J. Exp. Med. *130*, 619–642.

Pappas, L., Foglierini, M., Piccoli, L., Kallewaard, N.L., Turrini, F., Silacci, C., Fernandez-Rodriguez, B., Agatic, G., Giacchetto-Sasselli, I., Pellicciotta, G., et al. (2014). Rapid development of broadly influenza neutralizing antibodies through redundant mutations. Nature *516*, 418–422.

Potter, K.N., Li, Y., Mageed, R.A., Jefferis, R., and Capra, J.D. (1999). Molecular characterization of the VH1-specific variable region determinants recognized by anti-idiotypic monoclonal antibodies G6 and G8. Scand. J. Immunol. *50*, 14–20.

Sasso, E.H., Johnson, T., and Kipps, T.J. (1996). Expression of the immunoglobulin VH gene 51p1 is proportional to its germline gene copy number. J. Clin. Invest. *97*, 2074–2080.

Schroeder, H.W., Jr., and Dighiero, G. (1994). The pathogenesis of chronic lymphocytic leukemia: analysis of the antibody repertoire. Immunol. Today *15*, 288–294.

Schroeder, H.W., Jr., Hillson, J.L., and Perlmutter, R.M. (1987). Early restriction of the human antibody repertoire. Science *238*, 791–793.

Sela-Culang, I., Kunik, V., and Ofran, Y. (2013). The structural basis of antibody-antigen recognition. Front. Immunol. *4*, 302.

Steininger, C., Widhopf, G.F., 2nd, Ghia, E.M., Morello, C.S., Vanura, K., Sanders, R., Spector, D., Guiney, D., Jäger, U., and Kipps, T.J. (2012). Recombinant antibodies encoded by IGHV1-69 react with pUL32, a phosphoprotein of cytomegalovirus and B-cell superantigen. Blood *119*, 2293–2301.

Sui, J., Hwang, W.C., Perez, S., Wei, G., Aird, D., Chen, L.M., Santelli, E., Stec, B., Cadwell, G., Ali, M., et al. (2009). Structural and functional bases for broad-spectrum neutralization of avian and human influenza A viruses. Nat. Struct. Mol. Biol. *16*, 265–273.

Tang, X.C., Agnihothram, S.S., Jiao, Y., Stanhope, J., Graham, R.L., Peterson, E.C., Avnir, Y., Tallarico, A.S., Sheehan, J., Zhu, Q., et al. (2014). Identification of human neutralizing antibodies against MERS-CoV and their role in virus adaptive evolution. Proc. Natl. Acad. Sci. USA *111*, E2018–E2026.

Teplyakov, A., Obmolova, G., Malia, T.J., Luo, J., Muzammil, S., Sweet, R., Almagro, J.C., and Gilliland, G.L. (2016). Structural diversity in a human antibody germline library. MAbs *8*, 1045–1063.

Throsby, M., van den Brink, E., Jongeneelen, M., Poon, L.L., Alard, P., Cornelissen, L., Bakker, A., Cox, F., van Deventer, E., Guan, Y., et al. (2008). Heterosubtypic neutralizing monoclonal antibodies cross-protective against H5N1 and H1N1 recovered from human IgM+ memory B cells. PLoS ONE *3*, e3942.

Tu, C., Terraube, V., Tam, A.S., Stochaj, W., Fennell, B.J., Lin, L., Stahl, M., LaVallie, E.R., Somers, W., Finlay, W.J., et al. (2016). A combination of structural and empirical analyses delineates the key contacts mediating stability and affinity increases in an optimized biotherapeutic single-chain Fv (scFv). J. Biol. Chem. *291*, 1267–1276.

Vauquelin, G., and Charlton, S.J. (2013). Exploring avidity: understanding the potential gains in functional affinity and target residence time of bivalent and heterobivalent ligands. Br. J. Pharmacol. *168*, 1771–1785.

Watson, C.T., and Breden, F. (2012). The immunoglobulin heavy chain locus: genetic variation, missing data, and implications for human disease. Genes Immun. *13*, 363–373.

Watson, C.T., Steinberg, K.M., Huddleston, J., Warren, R.L., Malig, M., Schein, J., Willsey, A.J., Joy, J.B., Scott, J.K., Graves, T.A., et al. (2013). Complete haplotype sequence of the human immunoglobulin heavy-chain variable, diversity, and joining genes and characterization of allelic and copy-number variation. Am. J. Hum. Genet. *92*, 530–546.

Watson, C.T., Glanville, J., and Marasco, W.A. (2017). The individual and population genetics of antibody immunity. Trends Immunol. *38*, 459–470.

Wheatley, A.K., Whittle, J.R., Lingwood, D., Kanekiyo, M., Yassine, H.M., Ma, S.S., Narpala, S.R., Prabhakaran, M.S., Matus-Nicodemos, R.A., Bailer, R.T., et al. (2015). H5N1 vaccine-elicited memory B cells are genetically constrained by the IGHV locus in the recognition of a neutralizing epitope in the hemagglutinin stem. J. Immunol. *195*, 602–610.

Winter, G., Lobley, C.M., and Prince, S.M. (2013). Decision making in xia2. Acta Crystallogr. D Biol. Crystallogr. *69*, 1260–1273.

Wrammert, J., Koutsonanos, D., Li, G.M., Edupuganti, S., Sui, J., Morrissey, M., McCausland, M., Skountzou, I., Hornig, M., Lipkin, W.I., et al. (2011). Broadly cross-reactive antibodies dominate the human B cell response against 2009 pandemic H1N1 influenza virus infection. J. Exp. Med. *208*, 181–193.

Ye, J., Ma, N., Madden, T.L., and Ostell, J.M. (2013). IgBLAST: an immunoglobulin variable domain sequence analysis tool. Nucleic Acids Res. *41*, W34–W40.

Yeung, Y.A., Foletti, D., Deng, X., Abdiche, Y., Strop, P., Glanville, J., Pitts, S., Lindquist, K., Sundar, P.D., Sirota, M., et al. (2016). Germline-encoded neutralization of a Staphylococcus aureus virulence factor by the human antibody repertoire. Nat. Commun. *7*, 13376.

Ying, T., Prabakaran, P., Du, L., Shi, W., Feng, Y., Wang, Y., Wang, L., Li, W., Jiang, S., Dimitrov, D.S., and Zhou, T. (2015). Junctional and allele-specific residues are critical for MERS-CoV neutralization by an exceptionally potent germline-like antibody. Nat. Commun. *6*, 8223.